JOURNAL OF MATERIALS SCIENCE 31 (1996) 102–118

Evaluation and extension of physical property–porosity models based on minimum solid area

R. W. RICE
W.R. Grace & Co. Conn., 7379 Route 32, Columbia, MD 21044, USA
Consultant, 5411 Hopark Dr., Alexandria, VA 22310, USA

Physical property–porosity models based on minimum solid areas of idealized stackings of either: (1) spherical particles partially bonded (e.g. sintered), or (2) spherical pores in a solid matrix are shown to agree with appropriate physical property data for bodies whose porosity is reasonably represented by such stackings. Appropriate physical properties are those determined mainly by local stress or flux, e.g. elastic properties, strengths, and electrical and thermal conductivity. The minimum solid areas are, respectively, the: (1) bond (e.g. neck) area between particles defining pores smaller than the particles, or (2) minimum web thickness between adjacent pores being more than or equal to the surrounding particles (e.g. bubbles in a foam). Combinations of the models for mixtures of basic porosity types and changes in basic model parameters (e.g. stacking) over the significant porosity range covered, are shown to agree with the literature (mainly mechanical) property data for bodies of appropriate porosity combinations. Areas of further development and testing are noted.

1. Introduction

1.1. Background

Porosity is a pervasive and important microstructural factor in all materials because of its common, but variable, occurrence with variable and often significant effect on properties. Despite the obvious importance of porosity, much is still not well known, including a clear recognition and identification of which properties depend on which porosity parameters. Thus, there are some properties that have little, or no, dependence on porosity, mainly those determined primarily, or only, by the atoms present, their local bonding, or both. These include molecular weight and lattice parameter, with thermal expansion being an important macroscopic manifestation of the porosity independence of the latter. There are also some properties that depend primarily, or only, on the amount of porosity, i.e. the volume fraction porosity, P, i.e. they satisfy a rule of mixtures of the pore and solid phases. These are primarily properties that depend on the composition and mainly, or only, on the amount of mass present, because the volume fraction mass is simply $1\text{-}P$. Such properties include heat capacity, and dielectric constant and refractive index (provided special scattering or charging effects do not occur). However, most physical properties depend on both the amount of porosity and one or more aspects of the pore character. Defining and adequately measuring which other pore aspects are pertinent to various properties has been a major challenge in adequately defining, and hence predicting, the porosity dependence of many important physical properties. Properties that typically have such more complex dependence on porosity include mechanical properties and electrical and thermal conductivities.

The lack of predictive ability reflects the challenge of adequately addressing porosity–property relations, especially identifying those properties that depend on more than just P, and what the specifics of the additional porosity dependence are. Meeting this challenge requires simplification of the problem, but in a fashion that does not seriously distort or obscure the physical information being sought. Two approaches to modelling, and hence understanding, porosity dependence have been dominant for the very important area of mechanical properties. These are: (1) models based on pertinant cross-sectional geometries (discussed in Section 1.2, and the subject of this paper), and (2) micromechanics-based models. Particular attention in the latter has been focused on elastic properties [1–6], but such models have often been generalized to properties other than those for which they were derived. Thus, models based on specific elastic properties are often applied to other elastic properties, as well as strength (tensile and compressive) [4] and occasionally non-mechanical behaviour such as electrical and thermal conductivity [7].

As an illustration of some of the problems with such modelling, consider one of the most widely used micromechanics approaches [5]. This assumes that porous bodies conceptually be represented as being built up by packing of hollow spherical particles of an infinite range of sizes. The size of each particle and its central, spherical cavity or bubble are chosen so each particle has the same P as the resultant body to be modelled. The infinite size range is needed so that

0022–2461

smaller particles (of the same P) can fill all the interstices between larger particles, so there is no porosity in the body other than that from the central cavity in each particle. It is then assumed that the conceptual application of a hydrostatic pressure is uniformly felt by all particles so the resultant strain response can be calculated. A common approach to improving the agreement between these (and other) models is to let some parameter such as Poission's ratio be dependent on porosity, often in a physically questionable fashion, i.e. using it more as an adjustable parameter [5]. There are various questions about such models, including the extent to which stress concentrations play a role in porous materials, especially for elastic properties [8, 9]. However, of greatest concern for this modelling approach (and many other earlier models) is the neglect of the diversity of pore character by using a single type of pore to represent universally all pores. Generalization of the pores to spheroids [1, 2] does not help much because this still fails realistically to reflect many important pore types, as well as their combination, change, and variability discussed below.

Another reason for the lack of a predictive porosity–property ability is that all models have assumed a single type of porosity that remains fixed in basic character over the range of its applicability [1–7]. Thus, models assume that spherical pores remain spherical and that for pores between packed particles, which are determined by the packing, (i.e. stacking) of the particles retain the same stacking. Neither assumption of a single type of, nor a static, porosity is completely valid. Many porous bodies are much better approximated by a mixture of two or more idealized pore structures than a single one. An important combination is of the two basic types of porosity, i.e. of pores within and between particles, e.g. bodies made of hollow spheres. This is necessary because the only way to achieve $\geqslant 50\%$ porosity in a body of particles is to introduce some pores larger than those occurring between regularly stacked particles (because such porosity is inherently $<52\%$ in such structures). Even if one starts with a single idealized pore structure it will often change, for example, because particle stackings are generally not static as porosity changes, e.g. due to sintering. Thus, both cubic and orthorhombic particle stackings are unstable because they represent, respectively, the lowest and an intermediate stability of sphere location and of packing density [10]. For sintering solid particles, variations in size, deviations from spherical shape, multi-sphere stresses, or combinations of these can allow at least local shifts from cubic to orthorhombic or rhombic and from orthorhombic to rhombic stacking (i.e. lower particle stackings with lower coordination numbers, C_n, will be progressively less stable and, hence, more susceptible to rearrangements to increase C_n). Such increases in particle coordination numbers are basic to sintering, because green densities commonly imply particle $C_n \sim 6$–8, while grains in dense bodies typically have $C_n \sim 12$–14. Accounting for such changes again requires combining various models, but with the combinations changing with P. Many of these changes occur mainly at moderate to low porosity (e.g. <10–20% P) where their effects are limited. However, typically, pore stacking changes similar to particle stacking changes will occur, accompanied by pore shape changes at higher porosity levels, e.g. in foams, which can be more significant. Thus, surface tension commonly leads to some distortions of nominally spherical pores towards cylindrical pores (whose extensive intersection gives nearly cubic pores, e.g. as approximated in Fig. 2, see below) as P increases. Such progressive changes from spherical to cylindrical pore models need to be considered at high porosities. Thus, both common initial mixes of, and changes in, porosity make modelling of combined pore structures important.

A compounding problem in property–porosity studies is that the characterization of porosity, beyond an average P, is generally limited, or more commonly non-existent. While detailed porosity characterization is quite challenging, rudimentary characterization is limited, as is even basic processing information which may indicate some aspects of the porosity. However, some studies have been conducted where bodies with nearly ideal pore structures have been fabricated and some properties measured as a function of their level of porosity.

This paper is one of two papers directed toward a predictive capability for porosity-dependent properties depending on pore character. Both papers are based upon selection from, and combining of, a series of existing models based on the minimum solid area concept (discussed in Section 1.2). This paper summarizes these existing models based on a range of idealized pore structures and introduces their combination. Then literature data for porous bodies approximating these models are shown to be consistent with the corresponding model or combination of models. The companion paper [11] shows literature data for bodies having normal, i.e. non-idealized, porosity also to be consistent with these single or combined models for appropriate properties.

1.2. Minimum solid area models

Almost all pore structures can be obtained by (1) varying degrees of bonding (commonly by sintering) of various particles and packings defining and surrounding smaller pores, (2) using bubbles or fugitive particles to form solid webs or struts totally or partially enclosing each resultant pore (i.e. interchanging the pore and solid phases in case 1, or (3) combinations of these. Thus, reasonable idealizations of much porosity for modelling are regular stackings of identical spherical particles or bubbles. This translates into stacking of (whole or truncated) spheres contained within regular polyhedral, often cubical, cells (Figs 1 and 2). The limit of regularly stacked spherical particles is point contact with the containing polyhedra and each other, because, for a body to be a solid, it must have sphere-to-sphere contact. This typically limits such models $\lesssim 50\%$ porosity. Sphere sintering or bubble growth is accompanied by growth of the contact areas (which are usually at or near the poles and near or along the equator), and sphere truncation and accompanying

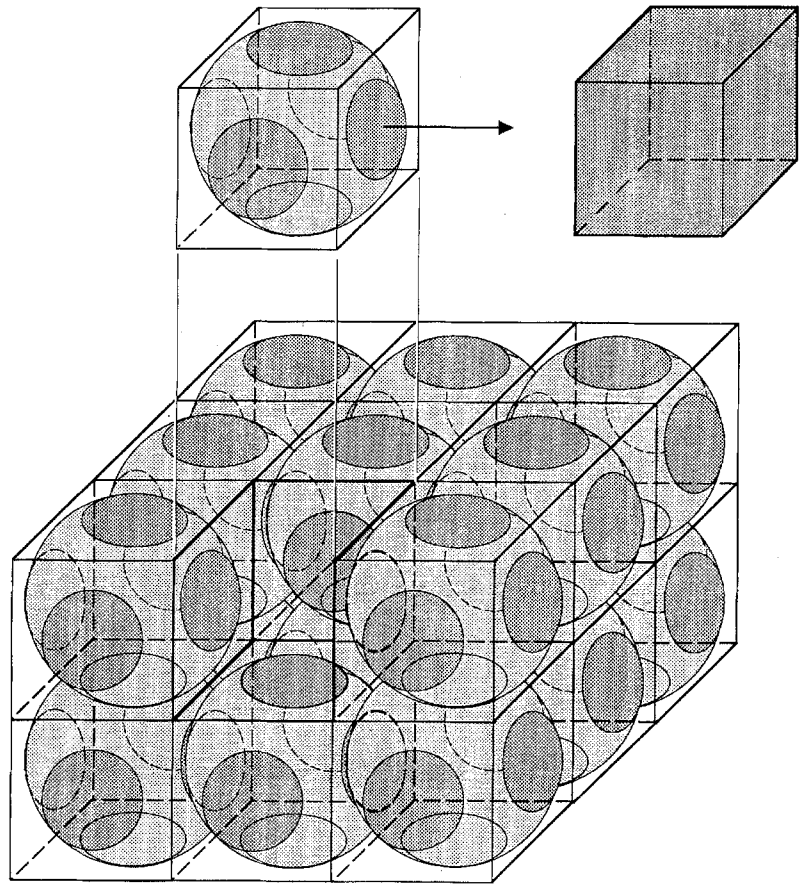

(a)

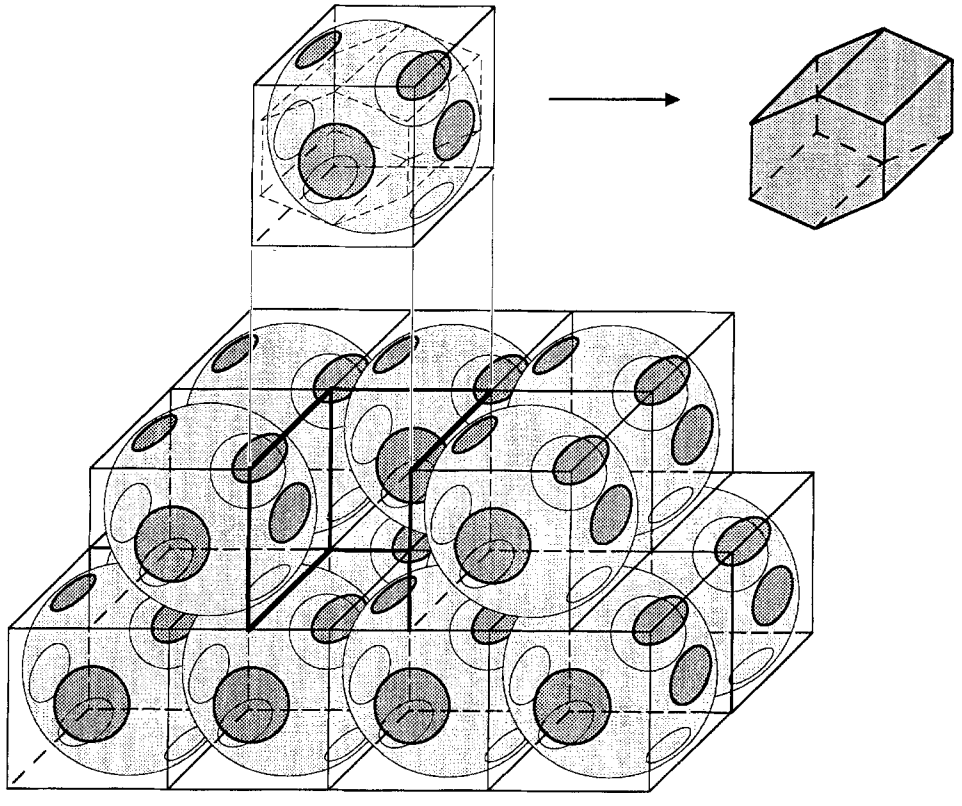

(b)

Figure 1 Idealized stackings of uniform solid spheres (or bubbles) in (a) cubic, (b) orthorhombic and (c) rhombic arrays. Note the circular or elliptical (due to perspective) area reflecting the minimum solid (bond) area for solid spheres (or degree of intersection of bubbles), and the resultant grain shape at full density for sintered spheres (the projected cell above the array), giving, respectively, (a) a cube, (b) hexagon and (c) dodecahedron.

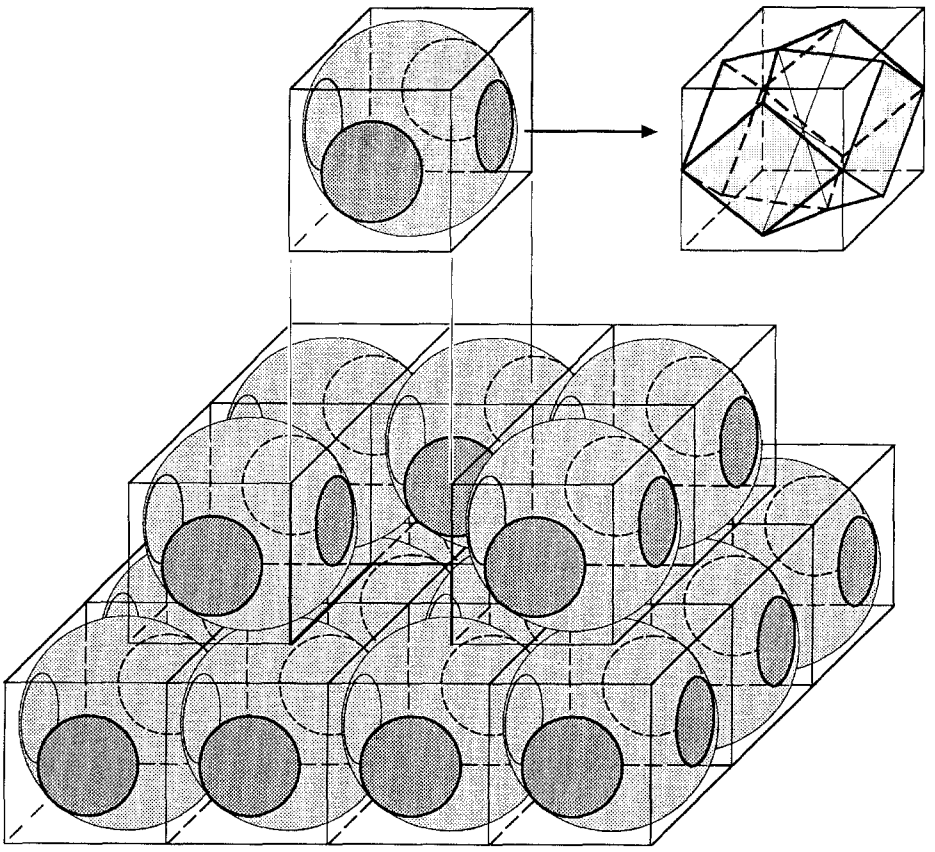

Figure 1 continued

shrinkage of both the polyhedra (whose sides always include the bond areas), and the body such that the volume of each resultant truncated sphere always equals the starting volume (i.e. conserving mass). The case of stacked bubbles, which is, in many respects, a mirror image of stacked spherical particles, can extend essentially over the full range of porosity, from zero through closed porosity to reticulated foams.

Many of the models for the porosity dependence of physical properties of ceramics and other materials have been derived using the above idealized structures to calculate actual solid cross-sectional areas. Typically the fraction of the zero porosity property values as a function of the volume fraction porosity, P, is equated to either the average or, more commonly, the minimum, fraction of solid area [6, 11–16] of the total body area normal to a reference (e.g. stress) axis. Minimum solid areas for stacked particles are the bond areas between them; for stacked bubbles the minimal solid areas are the minimal web cross-sectional areas between pores (Figs 1 and 2). Use of the average solid area is clearly logical for properties determined by a rule of mixtures of the properties of the solid and porosity (e.g. heat capacity), because the average area fraction of each phase equals its average volume fraction. An area basis is also logical for properties based on stress (i.e. elastic and strength behaviour), and flux (e.g. thermal and electrical conductivity) because these clearly also depend on the solid area. However, in these cases, the minimum, rather than the average, fractional solid area is more logically the controlling factor and has been most commonly used [6, 11–15]. The concept is that the minimum solid area normal to the stress (or conductive flux) should dominate the transmission of stress (i.e. strain, fracture toughness or energy, or strength) or conductive (thermal or electrical) fluxes through a body (e.g. Fig. 3). In a few special cases, the average and minimal solid cross-sectional areas are equal, e.g. for any type of long, parallel cylindrical or prismatic pores with the stress or flux parallel to the pore axis. Pore shape–stress concentration effects have also been used as a basis for mechanical property–porosity models [1, 6]. However, (1) the applicability of stress concentration effects to such porosity dependence has been questioned [8, 9], (2) minimum solid area has been shown to be more accurately correlated with properties than an accepted stress concentration model [8], and (3) interaction of pores reduces their stress concentrations, leaving the minimum solid areas as the main carrier of stress. Minimum solid area has also recently been shown to be the additional porosity parameter beyond the volume fraction (or per cent) porosity to characterize properties of porous solids which are not a simple rule of mixture of the amount of solid and porosity (e.g. of properties based on stress or flux) [10].

Minimum solid area models (though not necessarily labelled as such) have seen considerable development and use over the years for various individual pore structures, usually for mechanical properties. Thus, such models were developed for uniform spherical

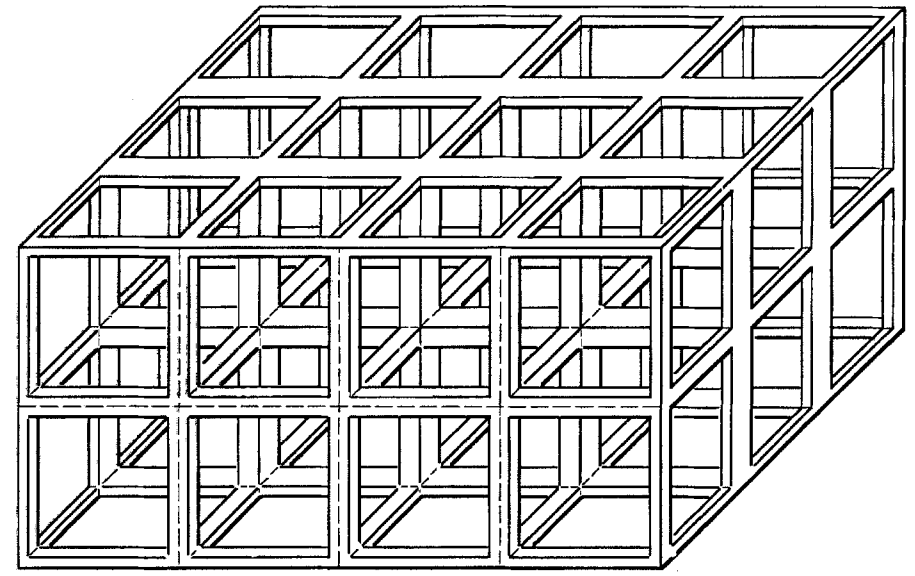

(a)

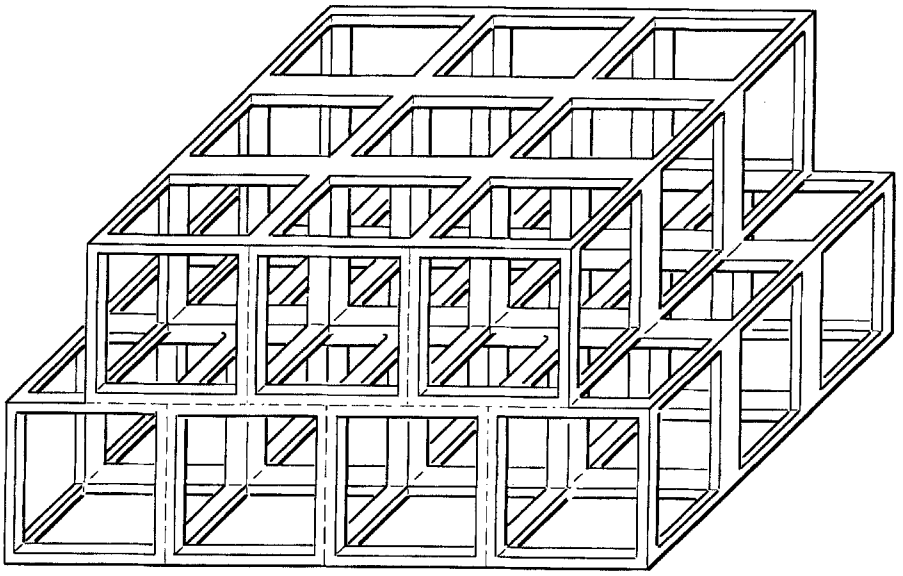

(b)

Figure 2 Idealized stackings of uniform foam cells, i.e. a much more extreme case of bubble intersections of Fig. 1 in the same stackings, i.e. (a) cubic, (b) orthorhombic and (c) rhombic. For simplicity of illustration, an approximately cubic void structure is used, when in reality, surface tension will increasingly determine the structure (see text), e.g. giving a pore shape close to something between first a truncated sphere and then a truncated cylinder as porosity increases. The minimum solid area is the web cross-section, which in reality will typically be tapered, usually to a minimum near its centre, due to surface tension.

pores [13], then cubical pores (stressed, normal to one set of cube faces [14], and subsequently for other orientations [6, 16]), solid spherical particles [12] (of simple cubic, orthorhombic, and rhombic stacking), and aligned cylindrical pores [15] (stressed parallel or perpendicular to the pore axis). Currently used models for various foam structures [17]) are essentially specialized minimum solid area models (using ideal structures like those of Fig. 2). Thus, they assume mechanical properties are determined by the properties and dimensions of the struts or webs between the pores rather than the thicker cross-sections, i.e. at the junctions of two or more webs or struts, which also neglects stress concentrations at such junctions. The solid spherical particle models were shown to be approximated over much of their lower P range by the exponential relation (e^{-bP}) with a given b value (i.e. slope of the initial approximately linear decrease on a semi-log plot, Fig. 4) corresponding to a given particle stacking, and hence pore structure [10]. This provided some theoretical justification for this exponential relation over its previously purely empirical use. Subsequently, all of the other above-noted minimum solid area models for other pore structures were shown to be similarly approximated by the exponential relation with b values, again corresponding to a given pore structure [6, 16], thus broadening the analytical basis for using the exponential relation. Also, the available collection of pore structures from minimum solid area models was shown to cover

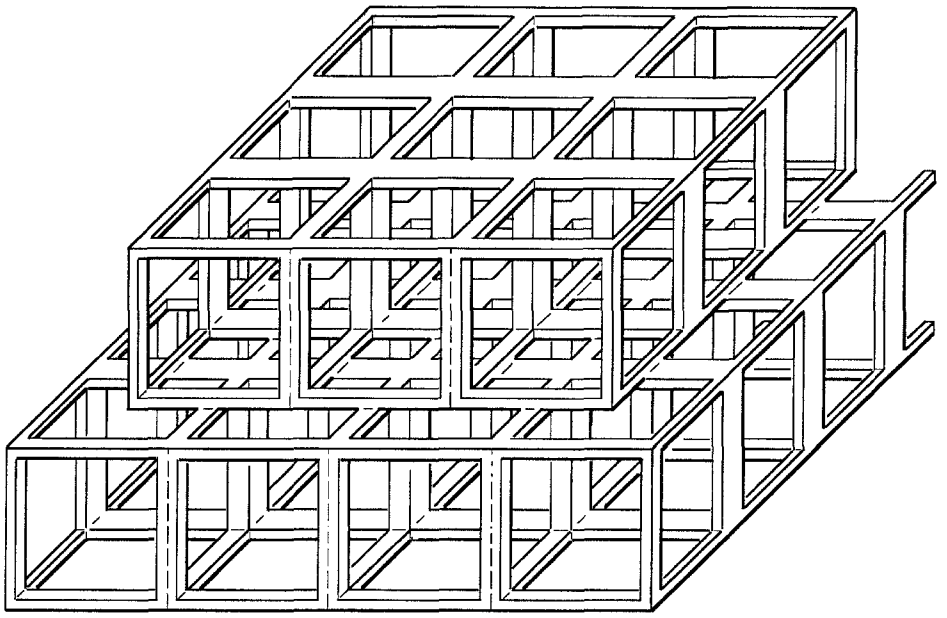

Figure 2 continued

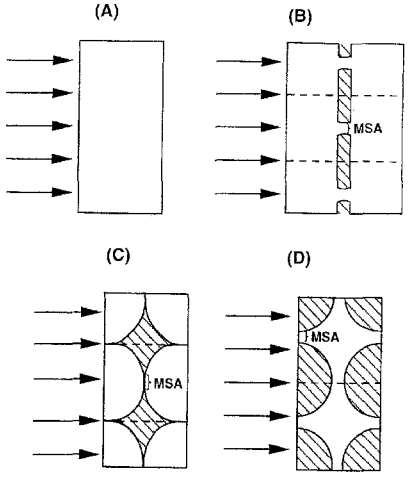

Figure 3 Schematic illustration of the minimum solid area concept. (a) The cross-section of a dense, uniform body where the transmission from layer to layer, normal to a uniform stress or conductive flux (e.g. electron or phonon), is the same in every layer; (b) the cross-section of a body identical to that in (a) except it has most of a layer removed, leaving only three small areas of continuity which now dominate the transmission of stress or conductive fluxes normal to the plane of the slab. Clearly, the average cross-sectional area is not a good indicator of the stress or flux transmission of this body; the limited contact areas, i.e. the minimum solid areas, are good indicators. (c), (d) cross-sections or particles or bubbles, respectively, where again the minimum areas of the solid cross-sections between pores (cross-hatched) will dominate stress or conductive flux transmission normal to the plane of the slab. Note horizontal dashed lines indicating basic, repeat cell structure of the bodies and designated minimum sold areas (MSA).

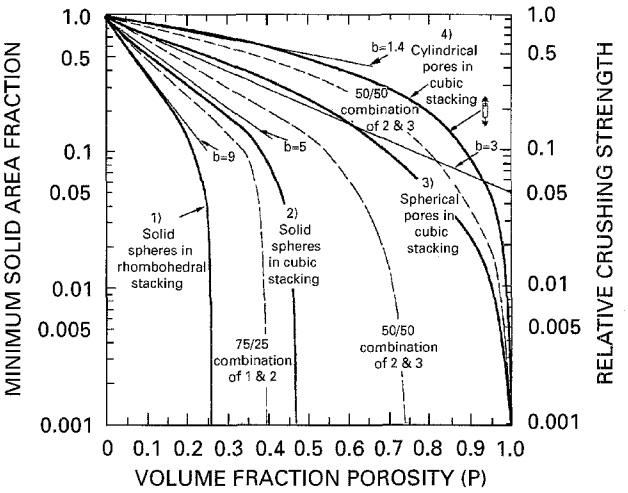

Figure 4 Models from the literature showing calculated ratios of minimum bond area per cell to the cell cross-section for the three basic sphere stackings (per Knudsen [12]), and for cubic stacking of spherical and cylindrical voids for stress or flux parallel or perpendicular (see arrow-cylinder sketches) to the axes of the aligned cylinders [15]. Note that the original plotting of the model for properties perpendicular to the axis of aligned cylindrical pores was significantly in error giving b or 7 and Pc or 0.2 [6, 15] in contrast to correct value of a 3 and 0.8 respectively, as shown. Note the rule of mixture combinations (– – –) for (a) 75% rhombically and 25% cubically stacked spherical particles, (b) 50–50 mixture of cubically stacked particles and bubbles (i.e. of hollow spheres), and (c) 50–50 mixture of cubic stacked spherical and cylindrical voids. For reference, slopes (i.e. b values of e^{-bp}) are shown as integer values of 1–9.

a sufficient range to model most, if not all, real pore structures [16]. Thus, minimum solid area models are applicable to a number of important physical properties, and have the important advantages of covering the entire P range and are effective (possibly unique) in allowing the diversity of pore structures to be addressed.

The minimum solid area models that are pertinent to this paper are shown in Fig. 4. Beyond the initial, approximately linear decrease of the minimum solid area (and hence the property value of interest) on a semi-log plot versus P, the property of interest starts decreasing more rapidly, then nearly precipitously, going to zero at a critical porosity, P_C. For stacked particles P_C, the percolation limit, is where the bond area between particles goes to zero. For pores (e.g. bubbles) in a matrix, it is the point at which the minimum web areas between particles goes to zero. Thus, each specific model has three characteristics: (1) the approximately linear slope of the first half to three-quarters of the P range to which it is applicable, (2) the

approximate P value at which properties start to decrease significantly more rapidly than the approximate linear slope, and (3) the P_C value. All three of these are useful in distinguishing the basic porosity character of each model, but their utility varies. Thus, P_C values are experimentally the least available, may be the most accurately defined theoretically and are not unique, e.g. they are the same for spheroidal and polyhedral pores having the same cross-sections as tubular pores of the same cross-section aligned parallel to the direction of property measurement. The approximate linear slopes are unique for basic models, and are the most widely available factor, giving considerable emphasis to them. The utility of each of the above three characteristics is further enhanced by combinations of different porosity, resulting in similar curves with the above three characteristic values given approximately by a weighted average of those for each type of porosity involved, as shown later (Fig. 4).

In addition to the above three characteristics of minimum solid area models to check them, they offer other opportunities for evaluating their applicability. As noted earlier, their minimum solid areas basis makes them applicable to not only stress determined (i.e. mechanical) properties, but also flux-determined properties, e.g. thermal and electrical conductivities. Thus, both mechanical properties and thermal and electrical conductivities as functions of P are evaluated as tests of the models. Another important test of them is their applicability to different materials, especially for mechanical properties. Thus, the assumption of these models is that mechanical properties are primarily determined by the minimum solid areas. This means that other aspects of pore shape that may effect factors such as stress concentrations not necessarily fully reflected in the minimum solid area are not dominant. Comparison of mechanical property–porosity behaviour of ceramics versus polymer and metals should thus be instructive because the typical absence of plastic deformation in ceramics allows them to sustain elastic stress concentrations, while plasticity in polymers and especially metals limits them. Thus, if stress concentrations are important they should result in a broader range of P dependence of mechanical properties in ceramics than in plastics, and especially metals. While this differentiation should be greatest for strength, it can also be applicable to elastic properties because, while a plastic or metal may macroscopically be in the linear elastic range, local stresses around pores can still exceed the yield stress.

It would be most desirable to model each of the entire curves in Fig. 4 with a simple equation that contains parameters readily relatable to the pore character so that one can understand the meaning of these parameters for combinations or changes of pore structures. One candidate for doing this is the equation proposed by Phani and Niyogi [18] giving the ratio of the property at some volume fraction porosity to that at zero porosity as

$$\left(1 - a\frac{P}{P_c}\right)^M \tag{1}$$

where a and M are constants for a given porosity. Phani has fitted this equation to the minimum solid area model for cubically stacked spherical pores in a matrix. Alternatively, one might use the similar equation derived by Shiller [19] which gives the property ratio as:

$$1 - a\left(\frac{P}{P_{P_c}}\right)^M \tag{2}$$

However, initial trials of these and similar combinations showed difficulty in fitting such equations to the various model curves. Thus, while one could obviously fit the porosity trends near their percolation limit well, this could not always reliably be done and also get a good fit to the lower porosity region. Further it is not clear that one could clearly associate the equation parameters with the porosity character in such model fitting. One of the basic problems with these equations is that the parameters all interact in one term of the equation. Also, while the P_C value would be an important parameter, it is often not available or is uncertain because data are often not carried to where the minimum solid area (and hence associated properties) start decreasing rapidly toward P_C, and even less are carried nearly to P_C.

Another approach is to utilize the approximately linear character on the semi-log plot over much of the porosity region to which the different individual models are applicable. This thus utilizes the commonly used exponential relationship where in the ratio of the properties at some porosity to that at zero porosity is given by

$$e^{-bP} \tag{3}$$

where b is a parameter determined by the character of the porosity (Fig. 4). This expression has been widely used for porosity studies in the past, first on an empirical basis, then on an analytical basis for different stacking of spherical particles [12] and various shaped pores in a matrix [6, 16] (for which other equations had been previously derived) [6, 13, 14]. This exponential expression has three basic advantages. First, it is a reasonable approximation for the actual models (prior to beginning the approach to P_C. (The fact that this is not an exact approximation is one of the reasons why some curve fitting may not always reflect it as fitting data as well as other models, especially if it is extended beyond its range of good applicability.) Second, there are extensive data for which the b values have already been determined. Third, it provides a single parameter, b, which can be correlated with pore character (e.g. Fig. 4) and can be readily adapted for pore combinations via a weighted average of the b values, as shown later. Further, because of this mathematical simplicity, it allows ready correlation of other properties. Thus, for example, because sound velocities are related to the square of the pertinent elastic moduli, b values for the velocities will simply be about half of that for the corresponding modulus. This exponential form, which will be used in this paper, also has potential for being combined with the similarly derived expression pertinent only for higher porosity

levels, which has the form [15]

$$1 - e^{-b'(1-P)} \tag{4}$$

This has been shown to have reasonable agreement with high P data, but is improved (and more accurate theoretically) by substituting P/P_C for P. Combination of this equation with 3 to cover the higher and lower P ranges would give, respectively, two independent parameters (b and b') besides P and P_C for potentially more versatile and accurate fitting of data. For the present paper, the focus will be on use of Relation 3 because this applies to most data of this study (and most literature data). However, where data cover most of the P range of a model, or the higher P range, it is compared to the appropriate model curve. Use of equation 4 is also illustrated.

2. Model combinations

The concept of combining various porosities in a body (via a rule of mixtures) was used in considering effects of heterogeneous porosity on properties and in evaluating porosity parameters in bodies with more than a single type of porosity [20]. It is also suggested by cubic and random stacking of particles yielding similar porosity [16] because the latter must involve some lower density (e.g. particle bridging) and higher density (e.g. orthorhombic or rhombic) packing to give the same porosity as simple cubic packing. However, neither broader combinations nor specific, quantitative methods of combining models have been considered.

Three methods of combining effects of different porosities are logical. The first is the rule of mixtures, i.e.

$$X = V_1X_1 + V_2X_2\,, \tag{5}$$

where V_1 and V_2 are the volume fractions of the two porosities (P_1 and P_2), X_1 and X_2 the respective material properties for these porosities, and X the resultant property. Such a rule of mixtures is an upper (Voight) limit, for example, for elastic properties (reflecting addition of elastic properties for slabs of two different materials stacked parallel to the applied stress, i.e. a parallel model). Second is a lower (Reuss) bound, for example, based on stressing slabs of two different materials stacked perpendicular to their plane of stacking (i.e. a series model)

$$X = \frac{X_1X_2}{V_1X_2 + V_2X_1}. \tag{6}$$

Because the values of any one property at $P = 0$ are the same for X, X_1, and X_2 these can be replaced by the relative values (i.e. the ratio of the property at any P to that of $P = 0$) in both of the above equations. The third method of combinations is to average the above two; i.e. the upper and lower bounds as is commonly done for elastic properties.

Each of the above combination methods has its known or potential uses (e.g. as noted above) and its uncertainties. The upper bound (rule of mixture) and the lower bound, and hence also their combination, give very similar values when the values of X_1 and X_2 are similar. The two methods give substantially different values of X when the values of X_1 and X_2 are far apart, e.g. when $X_1 \sim 0$, the upper bound gives $X = V_2X_2$, but the lower bound gives ~ 0. Which is closer to the actual value depends on the nature of the porosity, but for many such cases, it will be the lower bound, because pores often reflect a substantial series effect. Averaging the two may often be useful, but does not necessarily resolve the issue, because if one type of porosity gives ~ 0 properties, averaging it with a larger value is valid only if the series and parallel effects are approximately equal.

Examples of some of the basic models and their combinations (using Equation 1) are shown in Fig. 4. Because these involve combining similar levels of minimum solid area (hence also of pertinent properties) there are no significant differences whether the combinations were made via Equation 1 or 2. Families of such curves can thus be generated for various porosity combinations. Note that to at least a first approximation, such combinations result in a proportional combination of (1) the limiting porosity, P_c, values, i.e. when the contiguity of the body, and hence its properties, go to zero, and (2) the nearly linear slopes (b values of e^{-bP}) that are a reasonable approximation over the first half to three-quarters of the P range of the models being combined. Such combinations of model curves are thus logical, simple and effective. Some combinations of specific porosity will be considered. However, the above, more generic approach, i.e. using a family of combined model curves based on a weighted average of the appropriate basic model curves, from which pertinent members can be selected for each specific case, is used most extensively.

3. Comparison of model and experimental results

3.1. Bodies of mainly spherical or cylindrical pores in a matrix

Several sets of experimental results (mainly for mechanical properties) from the literature provide at least approximate checks on basic minimum solid area models. Hasselman and Fulrath [20] cast glass plates with up to 2.5% of essentially spherical bubbles of various sizes, giving a decrease of Young's modulus from $\sim 79.5 (P = 0)$ to ~ 75.5 GPa at $P = 2.5\%$ and similarly from ~ 33.3 to ~ 30.5 GPa for shear modulus. Cubic stacking of uniform spheres (which is very similar to random packing) would predict respective decreases to ~ 71.5 and ~ 30.0 GPa, i.e. in reasonable agreement, but somewhat greater decreases than observed. Variations in bubble size and distribution along with the limited porosity range (hence limited data) are probable factors in the limited differences between theory and experiment.

More definitive is the work of Walsh *et al.* [21], who sintered specimens from glass frit, obtaining 0%–70% P. Because the porosity was mostly closed, surface tension effects would imply that the pores were approximately spherical, especially at higher sintering temperatures (hence lower P). Their relative Young's moduli generally follow the spherical pore in cubic cell

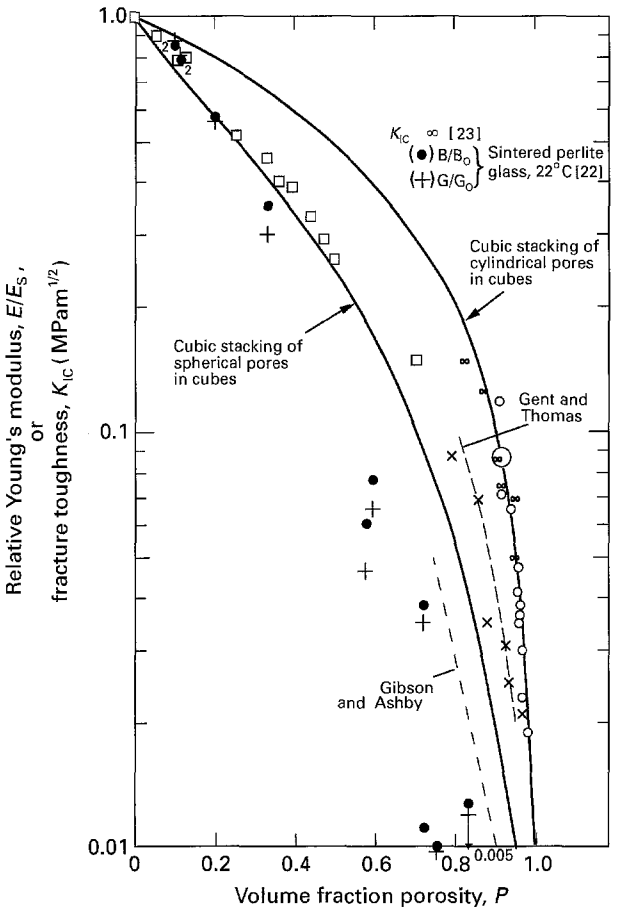

Figure 5 Plots of relative Young's modulus (i.e. of the porous body, E, divided by that of the dense body, E_s) and of fracture toughness versus volume fraction porosity, P, for sintered glass powders [21, 22] and for foamed glasses [23]. Note dashed lines showing fitting by Green [24] of foam-cell models of Gibson and Ashby [17] and Gent and Thomas [25] to E/E_s for the foamed glass. E: (□) [21], (○) [23] survey, (×) [23] measured.

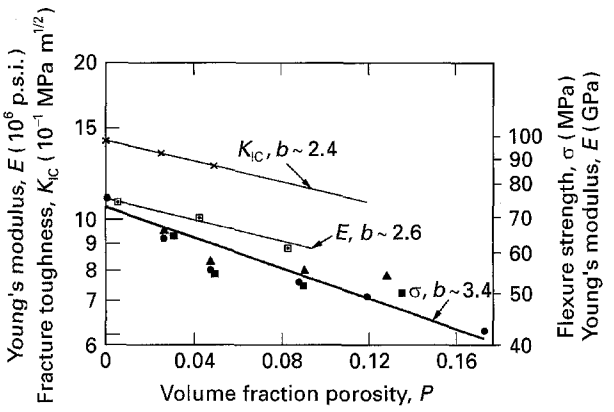

Figure 6 Data of Biswas [26, 27] for lead zirconate titanate (PZT) with mostly approximately spherical pores: (●) 25–40 μm, (▲) 60–75 μm, (⊡, ×, ■) 110–150 μm. Data for Young's modulus, E, fracture toughness, K_{IC}, and flexure strength, σ, shown versus volume fraction porosity at 22 °C, averaging b ~3 as expected from Fig. 3, with wider deviation for σ and especially K_{IC}.

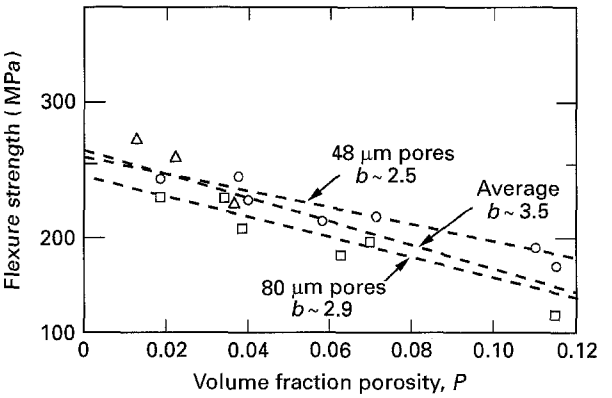

Figure 7 Flexural strength data of Wallace [28] for Al_2O_3 with mostly approximately spherical pores ((△) 28, (○) 48, or (□) 80 μm diameter) versus volume fraction porosity, P. Note b values average ~3 consistent with spherical pores, from Fig. 4.

model fairly well (Figs 4 and 5), consistent with random packing yielding very similar densities as cubic packing. Some deviation occurs at the highest porosity (P = 70%), consistent with possible changes from spherical toward cylindrical pores. Warren [22], sintering bodies from a pearlitic glass (with outgassing to also yield bubbles), obtained similar results. His relative elastic moduli also generally agree with the model for randomly stacked bubbles (Fig. 5). Deviation at higher P most likely reflects increasing residual porosity between incompletely sintered particles. Zwissler and Adams [23] summarized Young's modulus measurements for foamed glasses from various sources, and made their own measurements of Young's modulus and fracture toughness. Most of these measurements fall in between the curves for cubic (and hence approximately random) stacking of spherical and cylindrical pores, or on the latter, especially at higher P (Fig. 5), as expected. Also shown in Fig. 5 is the fitting by Green [24] of two foam-cell structure models [17, 25] for the relative Young's modulus, (E/E_s), of the foamed glasses. These data sets show the need for, and general agreement with, models covering a broad range of P.

Two cases of introducing spherical pores in polycrystalline bodies by incorporating rubber microspheres are shown in Fig. 6 (lead zirconate titanate) [26, 27] and Fig. 7 (Al_2O_3) [28]. Both show trends, i.e. log strength versus P slopes (b values) of ~3, reasonably consistent with that expected for cubic (hence also random) stacking of spherical pores. Somewhat higher b values than the spherical pore model are reasonable in view of the fact that there is also some residual grain-boundary porosity (which has higher b values, i.e. Fig. 4). Higher b values probably also reflect effects of heterogeneities. Considerable compressive strength data of glassy carbon [6, 29] where porosity should be predominantly spherical, gives a b value of 3.3 consistent with the model for spherical pores. Similarly, Young's modulus data for cast polymers with air bubbles [30, 31] show an average of b ~3 consistent with the model for spherical bubbles (Fig. 8). Variations probably reflect heterogeneities in the bodies.

More limited data for non-mechanical properties also support the models. Thus, plotting the log of thermal conductivity versus P of Al_2O_3 [32] at 22 °C (with pores of "roughly spherical or ellipsoidal" shape ~0.03 cm^{-1} diameter) gives b ~1.3 (Fig. 9). This is only approximately half the b value expected for

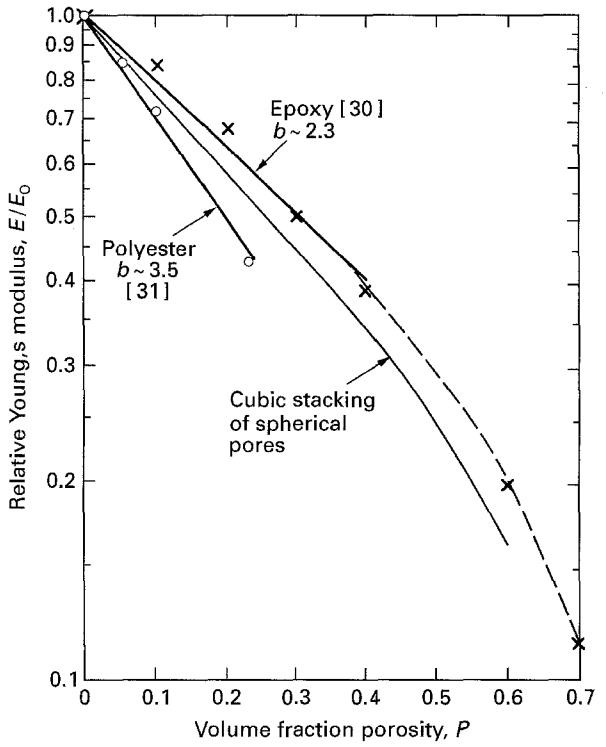

Figure 8 Relative Young's modulus versus volume fraction porosity for an epoxy [30] and a polyester [31] resin system with mostly approximation spherical pores versus volume fraction porosity, P, again giving an average b of ~3 consistent with Fig. 3.

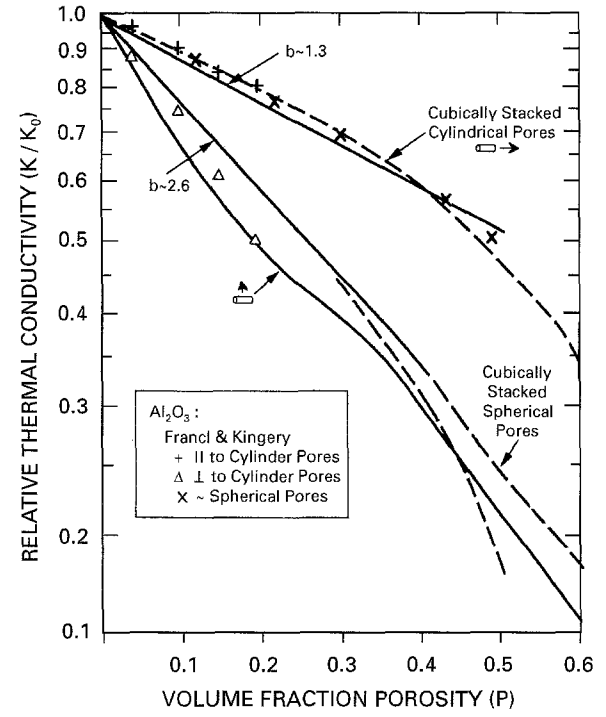

Figure 9 Relative thermal conductivity of Al_2O_3 with (×) larger, approximately spheroidal or oriented cylindrical pores (the latter tested both (+) parallel and (△) perpendicular to the cylindrical pore axes [32].

spherical pores. However, the quoted imperfect spherical shape (from expansion of naphthalene flakes volatilizing during early stages of firing in slip cast cubically shaped specimens) and the resultant b value would be consistent with pores approximated by-oriented cubes or cylinders [6, 15]. Conductivity parallel with aligned cylindrical pores (~0.082 or 0.146 cm diameter) in two Al_2O_3 bodies each gave a b value (i.e. slope) of ~1.1, i.e. 10%–20% lower but generally consistent with the corresponding model (Figs 4 and 9). Recognizing that there is also some added porosity from sintering, also lowering the conductivity improves the agreement. However, more important was the thick solid periphery around the sample (i.e. the cylindrical pore area constituted about 92%–94% of the specimen lateral dimensions). Thus, for testing parallel with the material around the cylindrical pores, there are four surface slabs of nominal sintered porosity (e.g. ~5%) conducting in parallel with the material with the cylindrical pores. Using the rule of mixtures (Equation 1) for these two porous materials for the highest porosity measurement ($P = 20\%$) gives a limited (e.g. ~10%) increase in the relative thermal conductivity from that of the theoretical prediction for the core section with the cylindrical pores to bring theoretical and experimental results even closer.

Thermal conductivity measurements normal to the above cylindrical pores in Al_2O_3 gave b values of ~3.5, i.e. only slightly higher than the model value of ~3 [6, 15] (Fig. 9). The modest discrepancy is partly attributed to the nature of the specimens. The large size of the pores (giving only 16 of the largest cylindrical pores across some specimens) may be a factor but, the peripheral slabs having only normal sintering porosity are again important. For measurement perpendicular to the cylindrical pores there are two slabs of nominal sintered porosity in series, and two in parallel, with thermal conduction normal to the cylindrical pores. Both sets of slabs would increase the thermal conductivity some due to their lower porosity, thus further increasing moded-data agreement.

A study of the compressive strength of sintered Al_2O_3 with cylindrical pores aligned parallel to the stressing direction, reinforces the above thermal conductivity tests and the overall modelling. Thus, Weiss *et al.*'s [33] data (Fig. 10) show the compressive strength initially dropping more rapidly as the number of axial cylindrical pores (~0.25 cm diameter) increases from 0 to 7, then fairly closely following the cylindrical pore model when 9 or more such pores are present. This initially more rapid decrease shows that a few larger pores are not sufficient to represent the model for such pores, i.e. supporting the above homogeneity issue (which is likely to be more serious for measurements perpendicular to the cylindrical pores). In fact, the initial slope (b value) of ~3.7 is a reasonable average of b values for axial cylindrical pores (b ~1.3) and pores between packed particles (b ~5–9, mostly 5–7). The trend for nine or more cylindrical pores decreases somewhat more rapidly than the ideal cylindrical pore model consistent with the presence of some residual porosity from sintering (~8%), and hence is in good agreement with the model.

Rutman *et al.* [34] measured electrical conductivity of sintered cubic ZrO_2 (+ 13% CaO) made with naphthalene additions giving approximate spherical

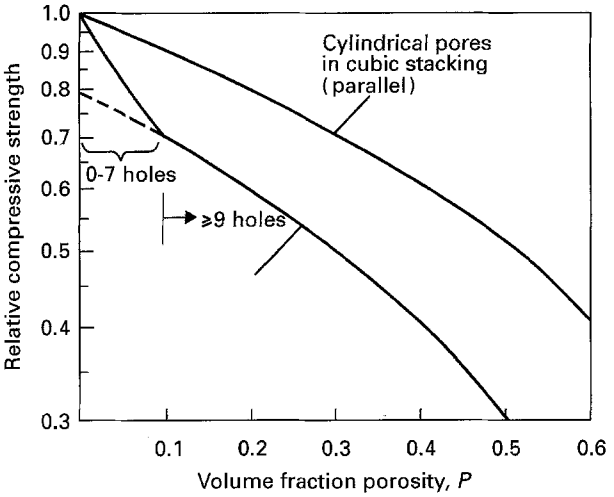

Figure 10 Relative compressive strength of Al_2O_3 with axial cylindrical holes. Data of Weiss *et al.* [33] at 22 °C for Al_2O_3 bodies sintered with 0–49 axial holes, ~2.5 mm diameter in parts ~2 cm × 2 cm × 5 cm. Rectangular bodies tested parallel to the aligned cylindrical holes. Note the change in slope going from 0–7 holes, with the curve for ⩾ 7 holes shown close to the theoretically predicted trend (upper curves).

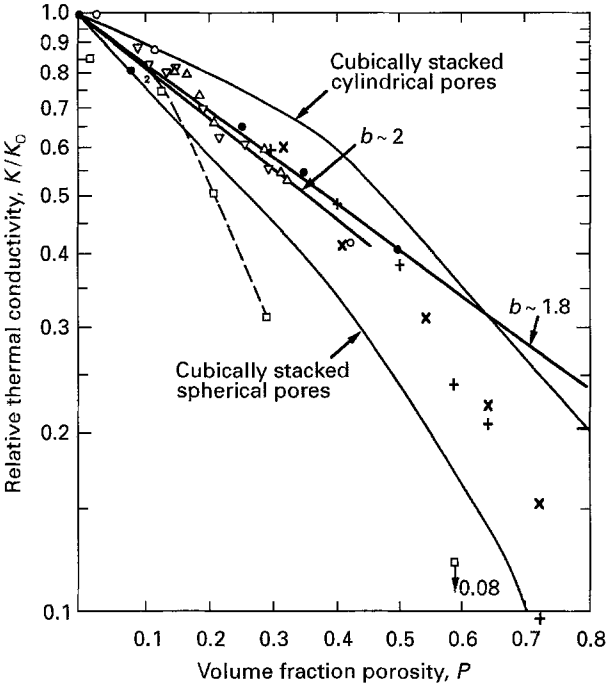

Figure 11 Relative thermal conductivity versus P (at 22 °C) for insulating bricks and rocks. Note that most exhibit low b values (2 ± 1) consistent with expected pores being spherical (e.g. from fugitive burnout) in the bricks, or lamellar or spherical in sedimentary rocks. (●) silicious marl [35], (×) SiO_2 brick [36], (+) diaspore brick [36], (○) limestone [37], (□) quartz-rich sandstone [38], ▽ Swaki sandstone [39] (△) Akabira sandstone [39].

porosity. Their b values for conductivity in the 800–1200 °C range are ~3, in good agreement with expectations. Similarly, thermal conductivity data for various sedimentary rocks and fire bricks [35–39] generally falls between the models for spherical and cylindrical pores (aligned with the conductivity direction, Fig. 11). The sedimentary rock data are expected to fall in this range because much of its porosity would be expected to be approximately spherical (e.g. due to air bubbles) and especially laminar (due to subsequent compaction of the lameller deposits giving laminar pores or porous areas) thus giving similar results to aligned, cylindrical pores. Similarly, fire bricks have much of their porosity as approximately spherical (or ore angular, e.g. approximately cubic pores from use of sawdust; cubic pores giving similar results as spherical pores [10, 15] thus generally following trends for spherical pores.

3.2. Bodies of solid or hollow spherical particles

Coronel *et al.* [40], measured Young's modulus, E, flexure strength, σ, and fracture toughness, K_{IC}, (using the notched beam technique) of bodies sintered from glass beads (averaging 100 μm diameter). Their E results (Fig. 12) show reasonable agreement with those expected for cubic (hence also random) stacking of uniform spheres. Less agreement is found, respectively, for σ and K_{IC}. Heterogeneities and their combination with the relatively large bead diameters are seen as major factors in these variations (e.g. as indicated by data range bars, Fig. 12). Orientation–anisotropy effects are probably also significant, especially for K_{IC} as discussed later, along with variations in flaw shape. McKinney and Rice [41] showed an approximate two-fold increase in K_{IC} values calculated from notch beam tests of dense glass bars due

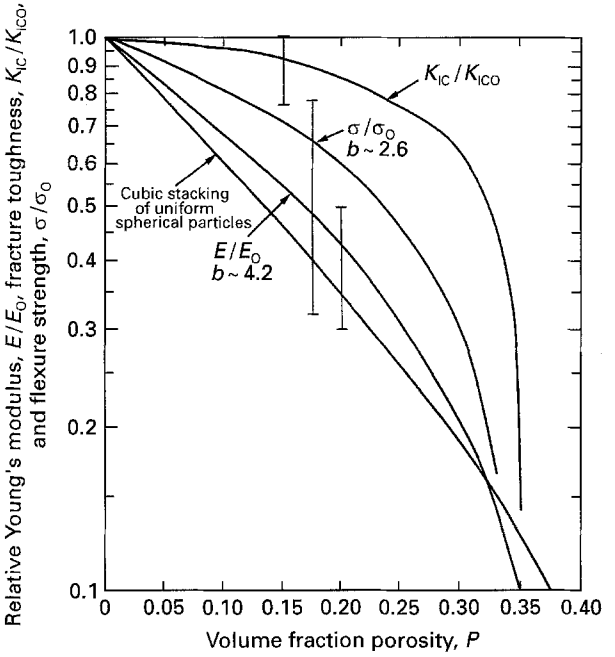

Figure 12 Relative Young's modulus, E/E_0, fracture toughness, K_{IC}/K_{ICO}, and flexure strength. σ/σ_0, data of Coronel *et al.* [40], versus volume fraction porosity, P, for sintered glass spheres at 22 °C. Note the greatest deviation of K_{IC} (but moderate range bar), and intermediate deviation of σ (but greatest range bar).

to flaws at the base of the notch being approximately semi-circular instead of highly elongated, i.e. approaching the slit crack assumed in notch beam calculations. Solid contiguity occurring only via necks between glass beads could readily limit machining crack

elongation at the base of the notch, making such variations in flaw shape more common in such porous glass bodies.

Bodies made by sol–gel processing are often closely approximated by stacking of spheres, e.g. as shown by the work of Ashkin *et al.* [42, 43]. Their E/E_0 data (Fig. 13) first closely follows that for cubic packed spherical particles (similar to that for random packing) up to $P \sim 30\%$, then approaches and crosses the curve for cubic stacking of spherical pores when the spherical particle stacking becomes very open (i.e. due to chains of spherical particles at $P \geqslant 50\%$), thus introducing a second population of pores, much greater than the particles. Thus, much of the higher level of porosity would be made up of approximately spherical, then cylindrical pores. Their (biaxial flexure) strength data show a similar trend, and agree quite well with earlier, more limited data of Park and Hench [44]. (Ashkin *et al.* show a rise in ν with increasing P, a trend not predicted by any model, which may often indicate heterogeneity in the porosity, [6] but the rise is limited.) Recent data on (uniaxial) flexural strengths of foamed gels by Fujiu *et al.* [45] also agree quite well with Ashkin *et al.* Finally, Woignier and Phalippou's [46] strengths (measured by both flexural and diametrical compression tests) of SiO_2 aerogels (as well as dense SiO_2 for reference) follow a similar, but higher trend. Their relative strengths (i.e. σ/σ_0) for both tests agree well with each other and generally fall between the models of spherical and cylindrical pores (Fig. 13). As might be expected, the data are closer to the cylindrical (cubic cell) model at the higher porosities, and closer to the spherical pore model at the lower porosities investigated.

Ali *et al.* [47], also sintered powdered glass, but with glass microballoons (~30–300 μm diameter) which made up the bulk of the resultant 0%–38% porosity. Their strength results again generally follow the trend predicted for spherical pores in cubes (i.e. $b \sim 3$, Fig. 14). Residual porosity in the sintered matrix is probably a major source of variations. A more extensive set of data for bodies made of glass balloons is that of Green and Hoagland [48, 49]. They used sodium borosilicate balloons sieved to give a limited size range (36 ± 11 μm) that were then sintered to various degrees with limited sphere damage, giving ~76% to ~92% porosity (determined by complete densification of balloon bodies). The lowest density, of course, was approximately the green density, which they determined to represent the spheres occupying ~52% of the volume (the remaining porosity was due to the pores inside the spheres). Their data for relative Young's modulus (E_s = the modulus of the solid, i.e. at $P = 0$, determined on specimens of fully densified balloons), flexural strength and fracture toughness are shown, along with three model curves, in Fig. 15. The first curve is for the function $1 - e^{-b'(1-P)}$ (with $b' = 0.5$) based on an earlier minimum solid load-bearing model [15] (derived by interchanging the solid and pore phase in the original minimum solid area model based on sintering spherical particles). This function has the right shape; its applicability can be improved by accounting for the green density, i.e.

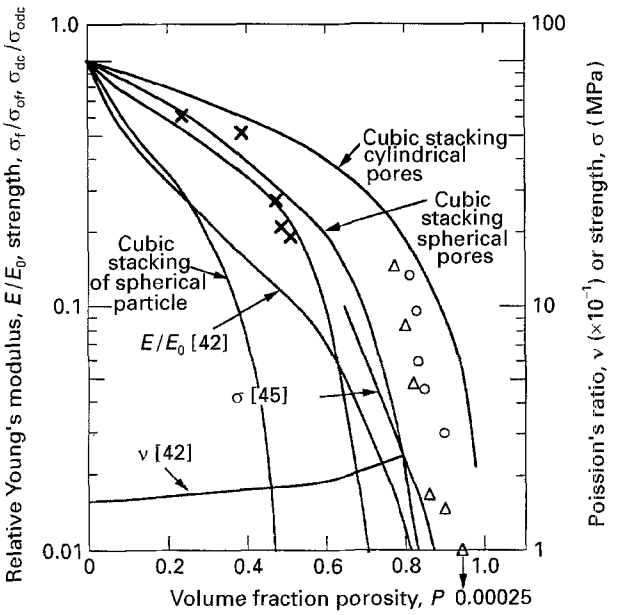

Figure 13 Plot of absolute or relative mechanical properties versus porosity, P, for bodies made from partially sintered gels [42, 43]. These bodies represent combinations of stacked sintering particles and bubbles and are generally consistent with such combined models. (×) σ [44], (○) σ_f/σ_{of} [46], (△) σ_{dc}/σ_{odc} [46].

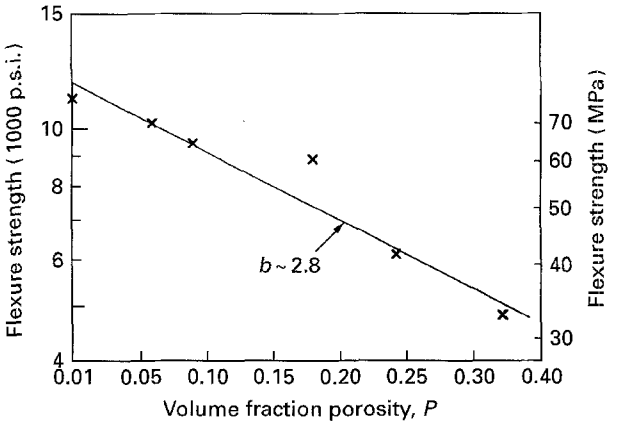

Figure 14 Flexure strength versus porosity, P, for sintered glass with balloons [47]. Compare slope, $b \sim 2.8$ to $b \sim 3$ for cubic stacking (Fig. 4) because random packing and cubic packing give very similar porosity–solid area curves and b values.

percolation limit, thus possibly being a useful component of more comprehensive modelling as noted earlier.

The other two model curves shown in Fig. 15 were derived by combining two minimum load-bearing models (for Young's modulus). One model used was based on the bond area between sintering spheres after that originally derived by Knudsen. Based on a green density of ~52%, the closest (cubic) sphere stacking having a limiting green density of ~48% was chosen to account for porosity between the balloons (spheres). The second model used was for the minimum solid area of spherical bubbles in a solid, e.g. after Eudier [13], and Rice and Freiman [6, 16], to account for the pores within the balloons. Combination of the two porosities and their effects was made via Equations 1 and 2, plotted for the sum of the two porosities, i.e. as suggested earlier by Rice [50]. As can be seen (Fig. 15),

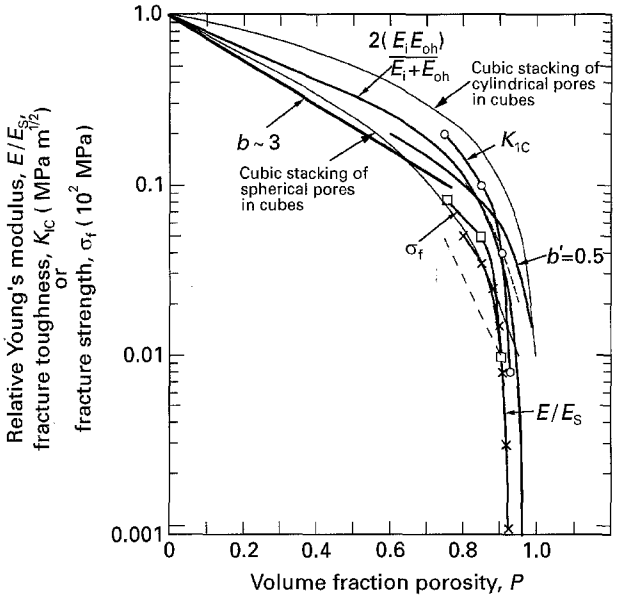

Figure 15 Plot of mechanical properties versus porosity, P, for partially sintered bodies of glass balloons after Green and Hoagland [48, 49] (×) E/E_s, (□) σ_f, (○) K_{IC}, and comparison to minimum solid area models for stacked bubbles. E = Young's modulus at any P (subscripts s = solid, i = values due to porosity inside of balloons, and o = values due to porosity outside, i.e. between, balloon). Note the lower bound $[2E_iE_o/(E_i + E_o)]$ which would be similar to the upper bound $(E_i + E_o)$. Also, the initial slope, $b = 3$ which reflects the approximate values for stacked spherical pores, and the fitting (---) of two foam cell models [17, 25] to these bodies by Green [24].

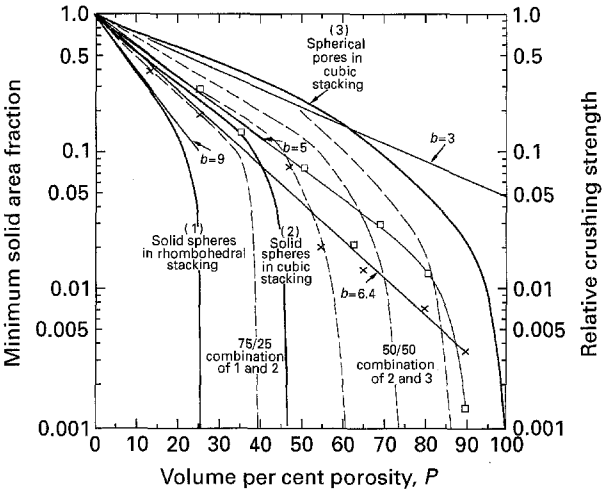

Figure 16 Crushing (compressive) strength data for Al_2O_3 and ZrO_2 bodies made from various mixtures of powder and polycrystalline balloons by Trostel [49], (×) ZrO_2, (□) Al_2O_3. Note the transition from cubic (approximately random) packing of solid spherical particle models to various mixtures of spherical voids (i.e. inside the balloons) to the limit of balloon addition (~75%)

the combined model fits the data reasonably well. The limited differences in absolute fit with the data must be due in substantial part to the difference in model versus actual green densities (48% versus 52%), as well as variability and imperfections in balloon size, shape and quality (e.g. broken balloons) and resultant uncertainties in the actual amount of each type of porosity. Also shown in Fig. 15 are the fitting by Green [24] of two foam cell models [17, 25] to their relative Young's modulus data, E/E_s. They noted that the data at higher P dropped below these models due to their properties being dominated by the small sintered contacts (i.e. their minimum solid area), and derived a model for such bodies accounting for these small contact effects [48].

Krasulin *et al.* [51] partially sintered bodies of various (sieved) size fractions of (6 wt%) CaO-stabilized ZrO_2 balloons from 20–200 μm in diameter. While the characterization of their balloons and resultant bodies is not detailed enough to allow significant quantitative evaluation, their data agree qualitatively and semi-quantitatively with the model. Thus, the decrease of various mechanical properties with increasing average balloon diameter is consistent in trend and approximate magnitude with predictions of the model, i.e. properties dropping by ~40% from the smaller to the larger balloon size. More definitive results from use of polycrystalline ceramic balloons is the work of Trostel [52]. He measured crushing strengths of Al_2O_3 and ZrO_2 bodies made by mixing and sintering powders with 0% up to ~75 vol % balloons (~2500 μm diameter). This broad range of hollow spheres provides a good opportunity to apply the preferred method of combination (Fig. 4). His data fall in the range for compacted spherical particles at lower P, i.e. zero or limited balloon content closest to simple cubic (hence also approximately random) powder packing (Fig. 16). Progressive addition of balloons results in maintaining the initial slopes (~5.1 for Al_2O_3 and ~6.4 for ZrO_2) well beyond the decrease of such solid particle packing models toward P_c. The agreement of the mixed powder–balloon bodies with the rule of mixtures curves from the cubic (approximately random) solid sphere and spherical void packing models support the preferred model combination approach discussed earlier.

4. Discussion

4.1. Model–data comparison

Comparison of literature data for bodies having pores approaching those readily modellable by minimum solid area models are consistent with the appropriate models. This is true not only for Young's, shear, or bulk moduli, but also for tensile (or flexure) and compressive (or crushing) strength, as well as thermal and electrical conductivities. The consistency for the limited number of cases for strengths and thermal and electrical conductivity as well as for polymer bodies of the paper is substantially reinforced by similar but more extensive consistency for these properties, as is the consistency of these with elastic moduli for a broader range of materials, including metals [11]. Both the overall consistency for this range of properties and materials provides good support for the minimum solid area concept. Consistency is also shown for the cases of mixed porosity and hence for the combination of porosities which is also further supported by the companion paper [11].

The term consistency used above is appropriate for two basic reasons. First, there are uncertainties in any modelling approach, such as the porosity simplifications and generalizations of micromechanics models

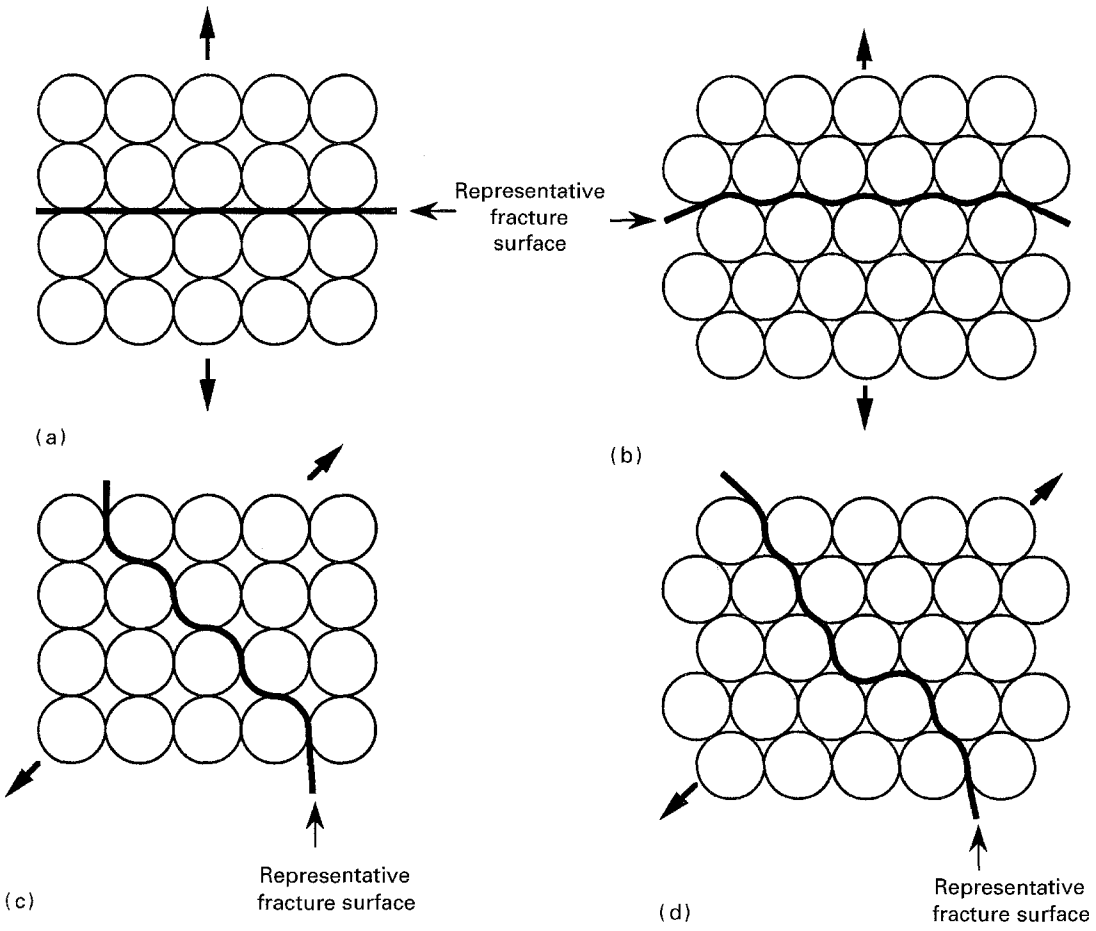

Figure 17 Illustration of variations in idealized fracture paths for various stackings of sintering solid spheres. Both (a) and (b) show, respectively, fracture paths for cubic and orthorhombic stackings stressed in the ⟨1 0 0⟩, and (c) and (d) show such paths for these two respective stackings stressed in the ⟨1 1 0⟩.

noted earlier. On the other hand, the minimum solid area models, while offering the widest range of porosity consideration, have the uncertainty of how dominant the minimum solid area is for various properties. Thus the use and possible validity of models can only be judged by extensive testing against property–porosity data. However, this poses the second basic problem; namely, the extent and quality of the data. No data exist (and would be very difficult to obtain) which very closely approach any available model. Further, while it is commonly assumed that porosity is homogeneous, where evaluations of this have been made they have shown substantial property variations, and hence implied inhomogeneity [6, 10]. These problems are compounded by the difficulties of detailed porosity characterization, and even worse, the common lack of even rudimentary characterization beyond measuring an average P. This and the companion paper [11] are the only known attempts to compare data for various pore types on any scale. Thus, micromechanics model evaluations have used far fewer case evaluations for support, and neglected the actual porosity character [1–7].

The issue of applying minimum solid area (or other) models to strength and fracture toughness needs to be further addressed. The most significant issue for tensile strength is the fact that pores may affect the flaw shape and especially the flaw size. However, as recently discussed [53], this occurs only in a fraction of the theoretical cases and is not observed to be a common factor experimentally [6, 53]. In most cases, flaws are much larger than the pores so the porosity dependence of strength, σ, is determined by $K_{IC} = (2E\gamma)^{1/2}$ (where γ is the fracture surface energy and E is Young's modulus). However, the P dependence of ν and E should be similar because theoretically the major determinant of γ is E [54]. The similarity of the P dependence of γ and E is frequently borne out [6, 16, 55]. However, there are also deviations, which are attributed to interactions of cracks, especially larger ones, with the pore structures as sketched in Figs 17 and 18 (discussed later). Bridging, or other larger scale crack–pore interactions, may result, giving these P deviations. However, the σ–P behaviour is much closer to E–P behaviour, showing much less, or no, manifestation of K_{IC}–P deviations [56]. This is also shown in this study, i.e. Figs 12 and 15, which also show similar E–P and σ–P trends, which thus further supports use of the minimum solid area models for σ [53].

Compressive failure entails propagation of cracks in local tensile stresses, hence, should have substantial similarity to σ–P behaviour as observed in this and other studies. However, compressive failure typically occurs by progressive, cumulative linkage of such local tensile cracks. There thus may be added opportunity for pore shape to have added effect on failure via effects on possible additional cracks generated at

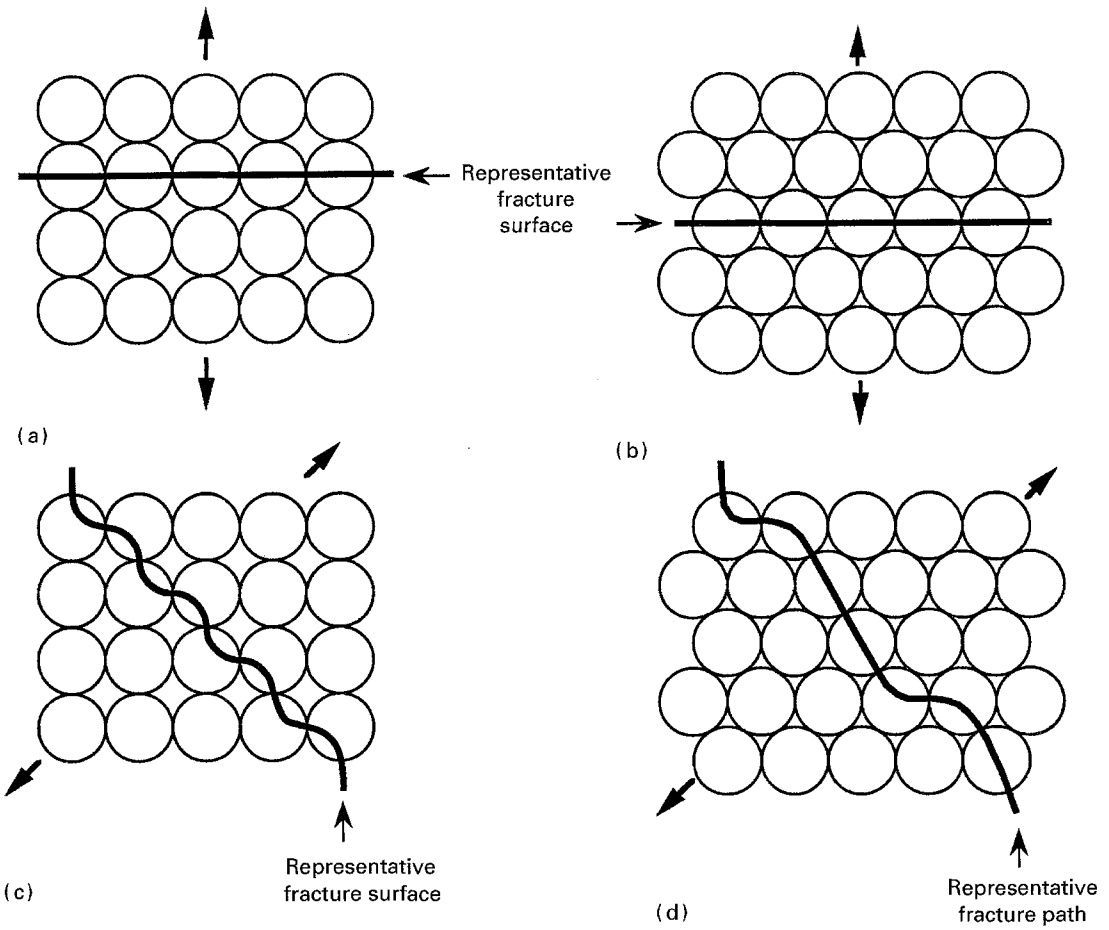

Figure 18 Illustration of variations in idealized fracture paths for various stackings of cells with bubbles in them. (a) and (b) show such paths, respectively, for cubes in orthorhombic stackings loaded in the ⟨1 0 0⟩. (c) and (d) show such paths for these respective stackings loaded in the ⟨1 1 0⟩.

pores as stresses increase beyond those where earlier cracks formed but did not cause failure.

However, the greatest need for improved model-data comparison in much more detailed characterization of the bodies at various stages of densification. As discussed further elsewhere [6, 10, 11], the most critical needs are to define the porosity better at which properties go to zero P_c, the contiguity of the solid phase (especially for bonded particles), and the homogeneity of the porosity. For bodies of sintered balloons, better characterization of the variations in balloon size and wall thickness are needed.

4.2. Further model development

This paper and its companion [11] show minimum solid area models are viable for dealing with many property–porosity situations. Their particular strength is their ability to address a variety of pore structures. However, there are three areas for further development, the first of which is further extension of the porosity range covered. Combinations of existing models based on uniform size and shape pores or particles have proved useful for handling real bodies. However, direct modelling of non-uniform size and shape pores or particles, e.g. using modern computational abilities, should be explored. There are also special porosities of importance for which direct modelling should be valuable. Varying pore structures obtained by leaching phase-separated bodies is one set of examples and preferential grain-boundary pores is another. Two other important categories are pores in composites (where interfacial pores between the matrix and dispersed phase are an important example) and pores in chemically bonded materials (e.g. plasters and cementitious materials).

The existing models can also be improved in two regards. The first is checking their isotropy. Minimum solid area models should not introduce any anisotropy or other non-uniformity not inherent in the basic material microstructure modelled. Use of spherical particles or pores in the three basic close packings of initially cubic cells (Figs 1 and 2) appears to result in isotropy, e.g. as suggested by the analogy with the corresponding cubic crystal structures based on identical stackings of atoms. Certainly isotropy results for all these models as $P \rightarrow 0$. However, isotropy has apparently not been considered before; for example, Knudsen's original calculations were of bond areas for three different sphere stackings (Fig. 4), but only for one direction, essentially ⟨1 0 0⟩, for each of these stackings [12].

In general, bond areas normal to the reference (e.g. stress, flux, etc.) direction play a major roll in supporting load, heat conduction, etc. Areas at intermediate angles play an intermediate role, and areas parallel to such direction a lesser role. Table I lists these three area categories for the three particle stackings and the three principal directions ⟨1 0 0⟩, ⟨1 1 0⟩, and ⟨1 1 1⟩. The geometry for making such analysis quantitative

TABLE I Qualitative summary of the angular variations for various stackings of bonded spheres. Number of bond areas perpendicular (I), parallel (II), or at intermediate angles (IA) to the reference axis.

Sphere stacking	⟨100⟩			⟨110⟩			⟨111⟩		
	I	IA	II	I	IA[a]	II	I	IA[a]	II
Cubic ($C_n = 6$)	2	0	4	0	6	0	0	4	2
Orthorhombic ($C_n = 8$)	0	4	4	0	4	4	0	8	0
Rhombic ($C^a = 12$)	0	8	4	0	8	4	0	12	0

[a]Intermediate angles α, i.e. $0° < \alpha < 90°$.

is relatively simple for simple cubic stacking. The projection of each bond area normal to the reference direction is an ellipse of area πab, where $b = a\cos(90 - \theta) = a \sin\theta$, and θ = the angle between the stress or flux direction and the plane of the bond area. The projected separation between like-oriented bond areas is

$$L = \frac{L'}{\cos(90 - \theta)} = \frac{L'}{\sin\theta} \tag{7}$$

where L is the actual separation in the plane of the bond, L' the separation projection normal to the flux (stress) direction, and θ is the angle of the reference (e.g. flux) direction relative to the plane of the bond area. The net bonding area, A, normal to the stress (or flux) direction is

$$A = \frac{2\pi a^2}{L^2}(\sin^2\phi_1 + \sin^2\phi_2 + \sin^2\phi_3) \tag{8}$$

where ϕ_i, $(i = 1, 2, 3)$, are the angles of the reference direction with the x, y, and z axes.

For the ⟨100⟩, ⟨110⟩, and ⟨111⟩ stress (flux) directions for cubic stacking, Equation 8 always reduces to $2\pi(a^2/L)$, indicating isotropy. (The same result is obtained for the minimum solid areas for cubic stacking of bubbles.) While increasing the packing density (i.e. C_n) for the other stackings increases the number of bonds, the angles between these and the reference direction decrease, again indicating a normalizing, hence isotropy trend, but more work is clearly needed.

The above observations indicating approximate isotropy are most pertinent to properties determined by non-destructive means, e.g. elastic, conductive, etc., properties. Properties determined by destructive means, i.e. fracture, are likely to show some perturbations or anisotropy because of fracture paths being biased toward the weakest areas (i.e. of the least solid bonding). Thus, some mixed-mode fracture on a local scale would be involved for some sphere stackings and stress directions, e.g. Fig. 17 as previously noted by Rice and Freeman [16]. This is most likely to manifest itself for bodies of limited sintering, i.e. higher porosity and for larger versus smaller cracks. This is consistent with K_{IC} data of Coronel *et al.* [40] showing greater deviation less than expected porosity decreases than for σ and this, in turn, less than E (Fig. 11).

Models based on stacking of bubbles, fully or partially, surrounded by solids have similarly not been thoroughly considered for the uniformity standpoint of essentially ⟨100⟩ stress or flux direction. While for foams, surface tension determines the structure, so the idealized structures of Fig. 18, especially of Fig. 18a and c, are not as realistic for their high porosities; they provide a starting point for illustrative purposes. Some mixed-mode failure on a local scale should occur in fracture of bodies of stacked bubbles (Fig. 18), introducing some anisotropy, mainly for more porous systems, especially if bubbles are greatly elongated along one direction.

The above issues associated with fracture illustrate the third area for further model development; namely better defining the applicability of these (and other) models. Minimum solid area models have broad applicability, for example to many mechanical properties and thermal and electrical conductivities. However, their applicability is not universal; for example, heat capacity and dielectric constant are primarily, if not exclusively, determined by average rather than minimum solid area. In some cases, it may be appropriate to modify minimum solid area models to account for other effects such as crushing in some wear tests [57]. In other cases it may be more appropriate to develop or apply other models, and to define which approach is most appropriate as discussed further elsewhere [11].

5. Conclusion

The applicability of existing models for the porosity dependence of physical properties determined mainly by local flux or stress and hence minimum solid bond (i.e. load bearing) area have been evaluated in two respects. First, the basic models are shown to agree with actual data for materials with porosity approximating the idealized pore structures of available models. Second, methods of combining porosity, thus covering a broader range of structures and a more complete range of porosity ($P = 0\%$ to nearly 100%), are discussed and shown to extend the applicability of the models. While direct combination of substantially differing property values from different porosities can be useful, further development is needed. However, different theoretical models can be combined where property values are similar, to yield combined model curves. It is shown that such combinations lead to approximate linear interpolations of the initial slopes and the value of the percolation limit, P_c, on a log property–porosity, P, plot. It is also shown that such combined models are in reasonable agreement with data for such combined porosities.

Acknowledgement

Mr Dan Wilhide, Technical Illustration Services, is thanked for preparing the figures.

References

1. R. ROSSI, *J. Am. Ceram. Soc.* **51** (1968) 433.
2. E. A. DEAN, *ibid.* **66** (1983) 847.

3. L. F. NIELSEN, *ibid.* **67** (1983) 93.
4. *idem, ibid.* **73** (1990) 2684.
5. N. RAMAKRISHNAN and V. S. ARUNACHALAM, *ibid.* **76** (1993) 2745.
6. R. W. RICE, in "Treatise on Materials Science and Technology 11," edited by R. McCrone, (Academic Press, New York 1977) pp. 199–381.
7. L. E. NIELSEN, *Ind. Eng. Chem. Fundam.* **13** (1974) 17.
8. R. W. RICE, *J. Mater. Sci.* **28** (1993) 2187.
9. *idem,* in press.
10. *idem, J. Am. Ceram. Soc.* **76** (1993) 1801.
11. *idem,* in press.
12. F. P. KNUDSEN, *J. Am. Ceram. Soc.* **42** (1959) 376.
13. M. EUDIER, *Powder Metall.* (9) (1962) 278.
14. B. PAUL, *Trans. Metal. Soc. AIME* **218** (1960) 36.
15. R. W. RICE, *J. Am. Ceram. Soc.* **59** (1976) 536.
16. R. W. RICE and S. W. FREIMAN, in "*Ceramic Microstructures,*" Vol. 76 edited by R. M. Fulrath and J. A. Pask (Westview Press, Boulder, CO, 1977) pp. 800–12.
17. L. J. GIBSON and M. F. ASHBY, "Cellular Solids, Structure & Properties" (Pergamon Press, New York, 1988).
18. K. K. PHANI and S. K. NIYOGI, *J. Mater. Sci.* **22** (1987) 257.
19. K. K. SCHILLER, in "*Mechanical Properties of Non-Metallic Brittle Materials,*" edited by W. H. Walton (Interscience, New York 1958) pp. 35–49.
20. D. P. H. HASSELMAN and R. M. FULRATH, *J. Am. Ceram. Soc.* **47** (1964) 52.
21. J. B. WALSH, W. F. BRACE and A. W. ENGLAND, *ibid.* **48** (1965) 605.
22. N. WARREN, *J. Geophys. Res.* **74** (1969) 713.
23. J. G. ZWISSLER and M. A. ADAMS, "*Fracture Mechanics of Ceramics,*" edited by R. C. Bradt, A. G. Evans, D. P. H. Hasselman and F. F. Lange (Plenum Press, New York 1983) pp. 211–42.
24. D. J. GREEN, "*Fracture Mechanics of Ceramics,*" Vol. 8 edited by R. C. Bradt, A. G. Evans, D. P. H. Hasselman and F. F. Lange, (Plenum Press, New York, 1986) pp. 39–59.
25. A. N. GENT and A. G. THOMAS, *Rubber Chem. Technol.* **36** (1963) 123.
26. D. R. BISWAS, "Influence of Porosity on the Mechanical Properties of Lead Zirconate-Titanate Ceramics", *Materials and Molecular Research Division Annual Report,* Lawrence Berkeley Laboratory, UCAL Berkeley (1976) pp. 110–13.
27. D. R. BISWAS and R. M. FULRATH, *Trans. J. Br. Ceram. Soc.* **79** (1980) 1.
28. J. S. WALLACE, "Effect of Mechanical Discontinuities on the Strength of Polycrystalline Aluminum Oxide", MS thesis, U. Calif. Berkeley, Lawrence Berkeley Laboratory, Materials and Molecular Research Division, Annual Report LBL-6016, UC-13, TID-4500-R65 Sept. 1978.
29. E. E. HUCKE, "Glassy Carbon", University of Michigan Report for Advance Research Projects Agency Order No. 1824 (1972).
30. O. ISHAI and L. J. COHEN, *Int. J. Mech. Sci.* **9** (1967) 539.
31. K. K. PHANI and R. N. MUKERJEE, *J. Mater. Sci.* **22** (1987) 3453.
32. J. FRANCL and W. D. KINGERY, *J. Am. Ceram. Soc.* **37** (1954) 99.
33. D. WEISS, P. KURTZ and W. J. KNAPP, *Am. Ceram. Soc. Bull.* **45** (1966) 695.
34. D. S. RUTMAN, A. F. MAURIN, G. A. TAKSIS and YU. S. TOROPOV, *Refractories* **5–6** (May/June) (1970) 371.
35. T. SAEGUSA, K. KAMATA, Y. IIDA and N. WAKAO, *Kagaku Kogaku* **37** (1973) 811.
36. J. B. AUSTIN, in "*International Symposium on Thermal Insulating Material.*" (American Society for Testing and Materials, Philadelphia, PA, 1936) pp. 3–67.
37. H. CLARK, "The Effects of Simple Compression and Wetting on the Thermal Conductivity of Rocks," *American Geophysical Union,* Reports and Papers, Tectonophysics, (1941) pp. 543–44.
38. W. WOODSIDE and J. H. MESSMER, *J. Appl. Phys.* **32** (1961) 1699.
39. A. SUGAWARA and Y. YOSHIZAWA, *ibid.* (1962) 3135.
40. L. CORONEL, J. P. JERNOT and F. OSTERSTOCK, *J. Mater. Sci.* **25** (1990) 4866.
41. K. R. MCKINNEY and R. W. RICE, "Specimen Size Effects in Fracture Toughness Testing of Heterogeneous Ceramics by the Notch Beam Method", Special Technical Publication 745 (American Society for Testing and Materials, Philadelphia, PA, 1982) pp. 118–26.
42. D. ASHKIN, R. A. HABER and J. B. WACHTMAN, *J. Am. Ceram. Soc.,* 73 CH. 1990 pp 3376–81.
43. D. ASHKIN, PhD thesis, Rutgers University (1990).
44. S. C. PARK and L. L. HENCH, *Sci. Ceram. Chem. Proc.* (1986) 168.
45. T. FUJIU, G. L. MESSING and W. HUEBNER, *J. Am. Ceram. Soc.* **73** (1990) 85.
46. T. WOIGNIER and J. PHALIPPOU, *J. Non-Cryst. Solids* **100** (1988) 404.
47. M. A. ALI, W. J. KNAPP and P. KURTZ, *Bull. Am. Ceram. Soc.* **46** (1967) 275.
48. D. J. GREEN and R. G. HOAGLAND, *J. Am. Ceram. Soc.* **68** (1985) 395.
49. D.J. GREEN, *ibid.* **68** (1985) 403.
50. R.W. RICE, *ibid.* **58** (1975) 458.
51. Y.L. KRASULIN, V.N. TIMOFEEV, S.M. BARINOV, and A.B. IVANOV, *J. Mater. Sci.* **15** (1980) 1402.
52. L.J. TROSTEL Jr, *J. Am. Ceram. Soc.* **45** (1966) 563.
53. R.W. RICE, *Mater. Sci. Eng.* **A112** (1989) 215.
54. J.J. GILMAN, in "*Fracture*", edited by B.L. Auerbach, D.K. Felbeck, G.T. Hahn and D.A. Thomas, (MIT Technology Press, Wiley, New York, 1959) pp. 193–224.
55. R.W. RICE, *J. Am. Ceram. Soc.* **77** (1994) 2232.
56. *idem,* to be published.
57. C.CM. WU and R.W. RICE, *Ceram. Eng. Sci. Proc.* **6** (1985) 977.

Received 19 October 1994
and accepted 15 August 1995